From argument of invariance under P, T we could predict that $\langle \mathfrak{s} \rangle$ is transverse and orthogonal to the 3-plane $\mathfrak{t}$, $\mathfrak{p}_b$, $\mathfrak{p}_\Lambda$ as if the Λ^0 were produced directly by $\pi^- + p^+ \to \Lambda^0 + K^0$. [The proof of Σ^0 production is given by

$$(M''\mathfrak{u}'' - M\mathfrak{u})^2 = M''^2 + m^2 - 2MM''\mathfrak{u}\cdot\mathfrak{u}'' \neq \mu_K{}^2]. \quad \text{(A.23)}$$

The asymmetry in Λ^0 decay even when the Σ^0 is not observed is therefore a measure of the function,

$$\frac{1}{2\pi}\int_0^{2\pi} \eta(\theta)\sin^2\varphi d\varphi,$$

of the polarization η of the Σ^0.

PHYSICAL REVIEW VOLUME 122, NUMBER 1 APRIL 1, 1961

π^- Scattering from Complex Nuclei*

R. M. EDELSTEIN,† W. F. BAKER,‡ AND J. RAINWATER
Columbia University, New York, New York

(Received November 29, 1960)

Differential cross sections were measured for π^--carbon scattering at 69.5 and 87.5 Mev and π^--oxygen scattering at 87.5 Mev from 20° to 125° extending the technique of Baker, Rainwater, and Williams. The energy resolution was sufficient to measure pure elastic as well as 5- and 10-Mev inelastic cross sections. The modified Kisslinger optical-model equation was used to fit the elastic-cross-section data. A χ^2 analysis for the 69.5-Mev carbon data gave a nuclear radius parameter $r_0 = 1.05 \pm 0.02$ fermis and a fall-off parameter $t = 1.16 \pm 0.07$ fermis. These parameters give good fits to the other data as well. An energy dependence in the strength parameters for carbon is observed in qualitative agreement with prediction.

I. INTRODUCTION

MEASUREMENTS have been made, using scintillation counters, of the angular distributions of π^- mesons scattered from carbon at 69.5 and 87.5 Mev and from oxygen at 87.5 Mev. The experimental work is an extension of that of Baker, Rainwater, and Williams[1] (BRW), in which the scattering of 80-Mev π^- mesons from Li, C, Al, and Cu was measured. In their experiment, scattered pion energy was determined from the range of pions stopped in a counter. This technique afforded considerable improvement in energy resolution over that obtained previously with counters[2–4] and cloud chambers.[5–7] The present experiment employed four such counters in succession, the "multicounter," to increase the data-taking rate. The energy resolution in either experiment was sufficient to separate out pure elastic scattering from all inelastic scattering for carbon and oxygen. In the case of lithium, BRW employ the electron scattering data[8] to argue that the contribution of scattering from the first excited state to the measured elastic scattering is small. No other levels contribute.

Recent experiments have been performed by Kane,[9] π^+ scattering from carbon at 31.5 Mev; and Fujii,[10] 150-Mev π^- scattering from C, Al, Cu, and Pb. Kane measured total pion energy by means of pulse height in a scintillation counter with an (absolute) energy resolution comparable to our own. Fujii measured quasi-elastic scattering into a 15-Mev interval by means of total energy determination in a Čerenkov counter but could not separate out pure elastic scattering.

Baker, Byfield, and Rainwater[11] (BBR) have fitted optical model calculations to the data of BRW. The optical potential used was a modification of the one of Kisslinger.[12] It removes a nonphysical divergence in the unmodified form. The potential includes a term in the gradient of the nuclear density which arises from the important p-wave contribution to the elemental π-nucleon scattering in the nucleus. Hence, the predictions are particularly sensitive to the nuclear edge thickness. The model gives good fits to the data at all angles and for nuclear radii consistent with the results

* This research is supported by the U. S. Atomic Energy Commission and the Office of Naval Research.

† Present address: Carnegie Institute of Technology, Pittsburgh, Pennsylvania.

‡ Present address: Brookhaven National Laboratory, Upton, New York.

[1] W. F. Baker, J. Rainwater, and R. E. Williams, Phys. Rev. **112**, 1763 (1958).

[2] A. Pevsner, J. Rainwater, R. E. Williams, and S. J. Lindenbaum, Phys. Rev. **100**, 1419 (1955).

[3] R. E. Williams, J. Rainwater, and A. Pevsner, Phys. Rev. **101**, 412 (1956).

[4] R. E. Williams, W. F. Baker, and J. Rainwater, Phys. Rev. **104**, 1695 (1956).

[5] H. Byfield, J. O. Kessler, and L. M. Lederman, Phys. Rev. **86**, 17 (1952).

[6] J. O. Kessler and L. M. Lederman, Phys. Rev. **94**, 689 (1954).

[7] G. Saphir, Phys. Rev. **104**, 535 (1956).

[8] J. F. Streib, Phys. Rev. **100**, 1797 (1955).

[9] P. P. Kane, Phys. Rev. **112**, 1337 (1958).

[10] T. A. Fujii, Phys. Rev. **113**, 695 (1959).

[11] W. F. Baker, H. Byfield, and J. Rainwater, Phys. Rev. **112**, 1773 (1958). Equations (2), (13a), and (13b) are printed incorrectly in this paper. The sign of the right side of Eq. (2) should be reversed. The expressions for C and C' in (13a, b) should be divided by A. In the present paper $C \to C_1$ and $C' \to C_0$.

[12] L. S. Kisslinger, Phys. Rev. **98**, 761 (1955).

of electron scattering.[13] The IBM-650 program of BBR has been used to fit the data of this experiment.

II. EXPERIMENTAL PROCEDURE

A. Detection Apparatus

The π^--meson beam used in this experiment was produced by the 380-Mev Nevis synchrocyclotron. The mesons were focused and deflected into the detection apparatus by means of a series of a dipole and three quadrupole magnets.

The detection apparatus was laid out as shown in Fig. 1. All counters were plastic scintillators and each was viewed by two RCA-1P21 photomultiplier tubes whose outputs were added. Counters 1, 2, and 3 were the incoming beam telescope. Counter 3, which was $\frac{3}{4}$ in.$\times$3 in., determined the target size. The carbon target thickness, 0.500 in., is equivalent to a 5-Mev loss of energy by an 80-Mev pion. The oxygen target was a container of water of thickness 0.750 in., the distance for a 5-Mev loss in water. The container was a light aluminum frame with 0.003-in. aluminum windows. $\frac{3}{8}$-in. thick slabs of Styrofoam were glued to the windows to maintain uniform target thickness. Thus, the total thickness of holder material in the beam was 5% by weight of the target thickness. The hydrogen contamination in the elastic scattering was small. The remaining counters and absorbers formed the scattered-beam telescope. Counters 4 and 5 detected pions of all energies scattered through angle θ, counter 5 defining the solid angle and the linear angle subtended by the scattered-beam telescope. The distance D_5 was varied from 40 in. at small values of θ to 12 in. at large angles—all other distances in the scattered-beam telescope remained fixed—to obtain maximum counting rate consistent with good angular resolution. The copper absorber slowed the pions so that most stopped in the "multicounter," counters 6 to 10, where pion energy was measured. The shield prevented all pions scattered in counter 3 from reaching the multicounter, except for $\theta \leq 30°$ where it could be only partially effective.

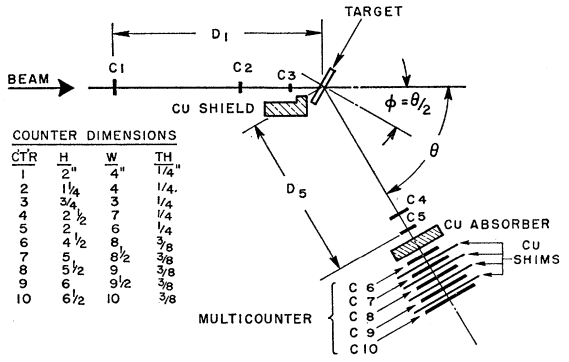

FIG. 1. Detection apparatus. Scattered beam telescope rotates in a vertical plane.

[13] D. G. Ravenhall, Revs. Modern Phys. **30**, 430 (1958).

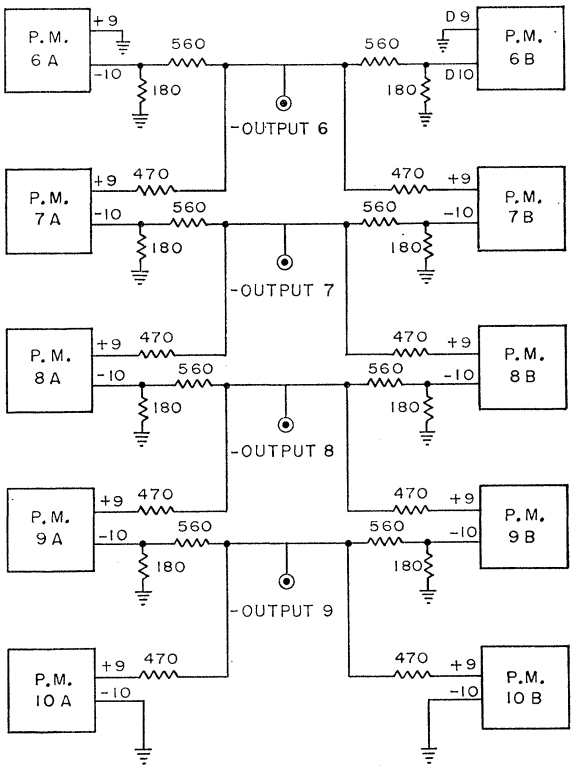

FIG. 2. Multicounter output circuit. Anticoincidences $\bar{67}$, $\bar{78}$, $\bar{89}$, $\bar{910}$ are made at the counters.

The remotely controlled scattering stand used was the one described in BRW. The scattered-beam telescope was mounted on an arm which rotated in a vertical plane. The target was always kept in a transmission-type geometry and rotated as the arm did to maintain $\phi=\frac{1}{2}\theta$. By this means, all π's scattered through θ traversed the same distance in the target, thus maintaining energy resolution. This geometry prevents measurements for $\theta \geq 125°$.

The multicounter was used to measure simultaneously four points on the differential range curve of the scattered pion beam by counting stoppings in counters 6, 7, 8, and 9. The technique is essentially the one described in BRW where, however, only one stopping counter was used. The scattered beam consists of a beam of elastically scattered pions and several inelastic beams, each corresponding to a particular excited final state of the nucleus. In the analysis, the justification for which is described in BRW, these several beams are replaced by an elastic and three inelastic beams whose mean energies are 5, 10, and 15 Mev less than the mean energy of the elastic beam. A beam is "centered" on a counter if the counting rate in that counter due to that beam is maximized. The shims were adjusted so that if the elastic beam was centered on counter 9, the other three beams were centered on 8, 7, and 6, respectively.

Stopped pions were identified by the technique em-

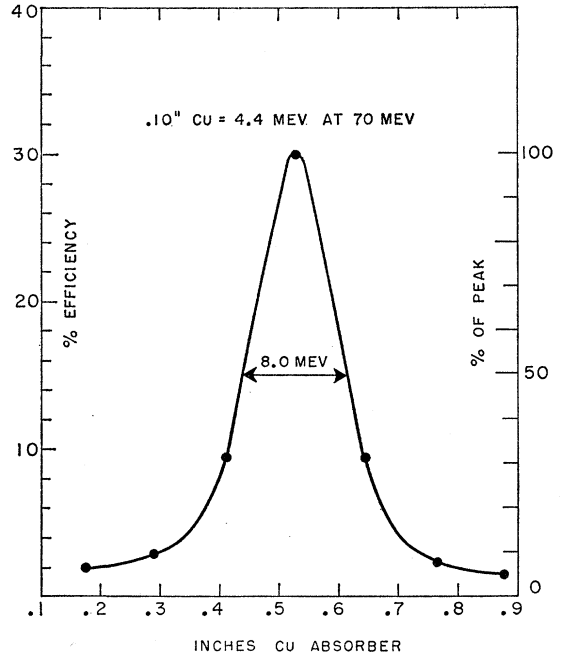

FIG. 3. Differential range curve for the 69.5-Mev beam (counter No. 9). Curve also represents efficiency of counter for beams of varying mean energy.

ployed in BRW. They give large light pulses both because of the stars produced upon stopping and the high rate of ionization at the end of the range. In addition to requiring a large pulse from a given counter for coincidence, anticoincidence was made with the succeeding counter. Figure 2 shows the layout of the anticoincidence circuits (simple subtraction circuits) used to make $6\bar{7}$, $7\bar{8}$, $8\bar{9}$, and $9\bar{10}$. Because of the nonzero energy resolution width, a beam which is centered on one counter gives counts in each of the others. Figure 3 shows the response of counter 9 to beams of varying mean energy. Similar curves were obtained simultaneously in the calibration runs for the other counters as well. These calibrations were made varying the absorber thickness, which is close to equivalent to varying beam energy. It is seen that the energy spread measured is ± 4 Mev. This same spread was obtained for both the 69.5- and the 87.5-Mev beam. The multicounter was calibrated every 24 hours and the drift was not sufficient to change the calculated cross sections by a statistically significant amount.

In view of the general usefulness of detectors for stopping π^- mesons, we may note that BRW originally tried using single detectors operated with sufficiently low voltages on the photomultipliers so that only very large energy release in the scintillator would be detected. The use of an anticoincidence member was found to give equally good energy resolution with greatly improved detection efficiency and improved operating stability. The photomultiplier tubes were still operated at reduced voltage but closer to the usual operating region.

The contributions to the over-all energy spread from the measuring process include the energy spread in the incoming beam, range straggling, stars produced in flight, scattering in the multicounter, and the energy interval corresponding to each counter thickness. The tight geometry after counter 5 and the graduated sizes of counters 6 to 10 tended to minimize beam losses due to multiple scattering in the Cu following counter 5. The other effects were necessarily present. In any event, the calibration of the multicounter, which measured the over-all effective spread, is all that is required in order to reduce the raw data. The individual contributions to the final spread need not be known since these were present both in the calibration and in the data-taking runs. Most important, the over-all spread is small enough to make feasible the separation of the elastic from the inelastic scattering for carbon and oxygen.

The equivalent copper thickness of the target was measured for each of the three differential cross-section curves during the initial calibration of the multicounter. The thickness of the copper absorber was altered for each value of θ so that the beam of elastically scattered π mesons was centered on an "elastic" counter, which for most runs was counter 9.

The energy of the elastically scattered π leaving the target is a function of θ for two reasons: nuclear recoil and the change in ionization loss of the π due to the increased slant distance traversed in the target by the π with increasing θ. The two effects are of comparable magnitude for the target thicknesses used. Plotted in Fig. 4 is $[E_\pi(0°)-E_\pi(\theta)]$ vs θ for the cases of interest including the hydrogen in the water. The proper copper thickness was calculated, accounting for the change of relative ionization with energy, and copper plates were specially ground to give an over-all error in absorber thickness of <0.005 in. of copper or <0.2 Mev.

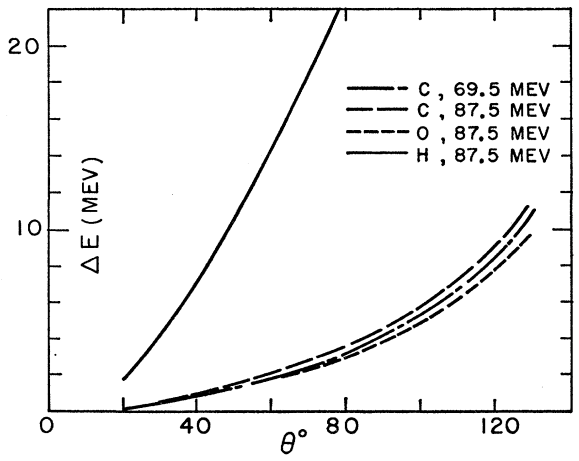

FIG. 4. Total loss of energy in target by an elastically scattered π vs θ. Loss is due to ionization and nuclear recoil. The O and H curves are for these elements in water.

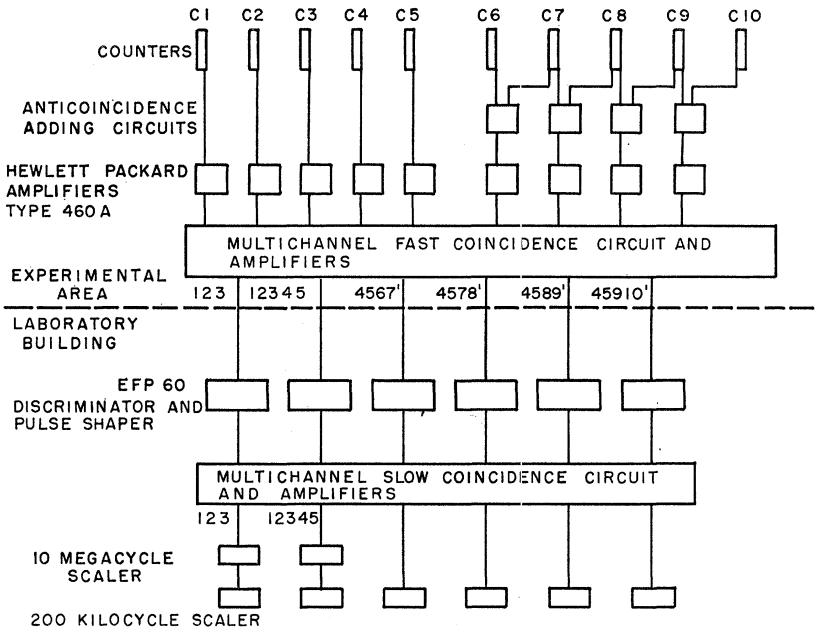

FIG. 5. Block diagram of electronics.

B. Electronics

The block diagram of the electronics layout is shown in Fig. 5. The coincidence circuits were all of Garwin type. It was necessary only to clip the counter pulses of high rate, counters 1, 2, and 3. The 1-2-3 coincidence then had a resolving time of 6 mμsec. Its accidental rate at the maximum coincidence rate of 11 000 counts/sec was 1%. The resolving time for the other 5 fast coincidences was 15 mμsec. The accidental rate in the multicounter coincidences was nil for $\theta \geq 35°$. However, it was found that the singles and coincidence rates in the scattered beam telescope were increased at small θ because these counters then intercepted part of the raw beam. The beam intensity was reduced at these angles so as to make the accidentals rate negligible.

The pulses from these 6 coincidence circuits were sent to the laboratory building to the EFP60 discriminator and pulse shaping circuits. The shaped pulse width was 80 mμsec; the dead time was 100 mμsec. These times, as well as the pulse height, remained essentially the same up to rates of 2×10^6 pulses/sec. The only significant dead time in the system was introduced in the 1-2-3 coincidence. The dead time correction was found to be 6% at a 1-2-3 rate of 10 000 counts/sec and to vary linearly with rate. A suitable correction is made to the cross sections.

C. Beams

The angular spread vertically after counter 3 of the beam defined by $C1$, $C2$, $C3$, was 4.5° full width at $\frac{1}{2}$ maximum. Helium-filled polyethylene bags were used to cut down air scattering. Their over-all effect cannot be stated, but a 25% increase in beam intensity was observed when the 18-ft long bag, external to the shielding wall, was put in place.

The lower energy beam was obtained by changing the radial and azimuthal positions of the cyclotron target from the positions for the 87.5-Mev beam. This lowered by 10 Mev the mean energy of the π beam which emerged from the shielding wall. The remaining 8-Mev decrease to 69.5 Mev was obtained by placing lithium and polyethylene absorber in front of counter 1. Quoted beam energies are at the center of the target when $\theta=0°$. The 1-2-3 counting rates for the 2 beams during data taking were 9000/sec at 87.5 Mev and 3000/sec at 69.5 Mev. The reduction in rate for the lower energy beam was essentially due to multiple scattering in the additional absorber. These rates include the μ and e contaminations which total 10–15%. It is not necessary to know this contamination precisely since these particles were not counted in the multicounter in the calibration runs because of their range, and they were not present in the scattered beams.

III. DATA PROCESSING

Differential cross sections for elastic and 5-, 10-, and 15-Mev inelastic scattering were unfolded from the stopping rates measured in counters 6, 7, 8, and 9. The method used is described in BRW. Calculations were carried out using the IBM-650 computer. The result of the unfolding process is a well-determined elastic cross section and inelastic cross sections which give a good indication of the cross sections for scattering from the low-lying excited levels of the nucleus. Both carbon and oxygen are well suited to this method as a large separation in energy exists between the ground state and the first excited state.

The first several levels for carbon are 4.43, 7.66, and 9.63 Mev with 8 levels between 10 and 15 Mev; while for oxygen they are 6.06, 6.14, 6.92, 7.12, 8.88, 9.58, and 9.84 Mev, with 17 levels between 10 and 15 Mev.[14]

At the small angles, it was possible to combine the counts of counters 9 and 8 to measure elastic cross sections without unfolding, since at angles $\theta \leq 55°$ the inelastic scattering was negligible. By this means, errors on the small-angle data were reduced. This is justified by the extended runs taken at 40° which showed inelastic cross sections that were effectively zero, and by the general trend in inelastic scattering observed at larger θ. Furthermore, the two methods gave the same result at small angles.

There are several small corrections to these cross sections which must be considered:

1. π decay in flight. The system was always calibrated with $(D_5)_{\min}=10$ in. Runs were taken with various values of D_5 from 40 in. to 12 in. Therefore, there were varying amounts of π decay in flight. Detailed considerations show that the decay muons give negligible contribution so the decayed π must be considered "lost." An appropriate small correction is made for this effect.

2. Angular spread. The angular spread of the beam incident on the target was measured to be 4.5° full width at half maximum for both beams. The angular spreads listed with the data also include the effects of multiple scattering in the target and of the angle subtended by the defining counter ($C5$) at the target position. Rather than alter the data, the angular spread was folded into theoretical cross-section curves which were fitted to the data. A Gaussian distribution in angle was assumed.

3. Change of calibration with θ. The energy of the scattered beam decreases with θ. The copper absorber was decreased correspondingly so that the elastic beam was always centered on counter 9. However, each counter thickness corresponded to a slightly larger energy interval since the specific ionization was increased. Effectively, the efficiency of the whole multicounter increases with θ. The increase is $\sim 3.5\%$ at $\theta=120°$ for C and O.

4. Hydrogen contamination. The π^- scattering from hydrogen in the water must be accounted for only at the smallest angles in the oxygen scattering. From Fig. 4 it is seen that the energy loss of a π scattered from a proton increases much faster with increasing θ than for a π scattered from oxygen. A correction $<2\%$ is made to the measured elastic count for $20° \leq \theta \leq 30°$. For $\theta \geq 35°$, hydrogen scattering groups with the inelastic scattering from O.

TABLE I. Differential cross sections (in mb/sr) of carbon for 69.5-Mev π^- mesons.

θ	Elastic	5-Mev inelastic	10-Mev inelastic
20±3.1°	147 ±16		
25±3.1°	93 ± 9		
30±3.1°	79.1 ± 6.6		
35±3.1°	50.5 ± 4.7		
40±3.1°	41.5 ± 3.5		
45±4.0°	26.9 ± 2.0		
50±4.0°	14.9 ± 1.2		
55±4.0°	8.9 ± 1.0		
60±4.0°	5.08± 0.56	0.58±0.56	0.31±0.48
65±4.0°	4.15± 0.33	[a]	0.12±0.29
70±4.7°	3.21± 0.25	[a]	0.44±0.25
75±4.7°	4.06± 0.31	[a]	0.41±0.25
80±4.7°	4.48± 0.71	0.66±0.68	[a]
85±4.7°	4.89± 0.50	0.76±0.45	[a]
90±4.7°	5.07± 0.83	[a]	[a]
95±4.7°	5.23± 0.32	1.04±0.32	1.22±0.29
100±4.7°	5.34± 0.62	1.81±0.65	0.53±0.54
105±4.7°	4.38± 0.53	1.58±0.58	1.39±0.52
110±4.7°	4.91± 0.58	2.35±0.65	1.44±0.58
115±4.7°	3.37± 0.48	2.68±0.60	1.61±0.56
120±4.7°	3.16± 0.47	3.39±0.61	1.54±0.57
125±4.7°	2.16± 0.44	3.70±0.64	3.18±0.63

[a] Unfolds to negative cross sections.

TABLE II. Differential cross sections (in mb/sr) of carbon for 87.5-Mev π^- mesons.

θ	Elastic	5-Mev inelastic	10-Mev inelastic
25±2.8°	109.2 ±10.6		
30±2.8°	86.0 ± 6.1		
35±2.8°	68.4 ± 4.9		
40±2.8°	39.8 ± 1.8		
45±3.8°	29.0 ± 2.6		
50±3.8°	15.0 ± 1.0		
55±3.8°	7.79± 0.51		
60±3.8°	5.80± 0.49	0.53±0.48	0.24±0.38
65±3.8°	4.18± 0.34	0.45±0.33	0.08±0.27
70±3.8°	3.46± 0.29	0.07±0.30	0.39±0.27
75±4.5°	3.63± 0.26	0.05±0.25	0.32±0.21
80±4.5°	4.07± 0.44	0.19±0.37	0.24±0.31
85±4.5°	3.57± 0.51	0.73±0.47	0.36±0.38
90±4.5°	3.30± 0.30	0.96±0.32	0.65±0.28
95±4.5°	2.78± 0.40	1.01±0.42	1.07±0.39
100±4.5°	2.60± 0.31	1.53±0.37	1.72±0.36
105±4.5°	1.72± 0.26	1.67±0.33	1.77±0.33
110±4.5°	1.16± 0.23	1.97±0.33	2.08±0.34
115±4.5°	0.80± 0.29	2.38±0.49	2.07±0.50
120±4.5°	0.90± 0.28	2.03±0.47	2.66±0.51
125±4.5°	0.61± 0.26	2.41±0.45	2.25±0.47

IV. EXPERIMENTAL RESULTS

Differential cross sections for the three sets of data are listed in Tables I, II, and III. Included in each table are elastic and 5- and 10-Mev inelastic cross sections with their statistical errors. The small-angle elastic cross sections, $\theta \leq 55°$ are the nonunfolded ones. Therefore, no inelastic cross sections are listed for this region. These results are shown graphically in Figs. 6, 7, and 8. The theoretical fits to the elastic scattering data shown on these graphs are discussed below.

The ratio of the inelastic to the elastic cross section increases steadily with increasing angle, energy, and nuclear size. Thus, at the largest angles, they are of comparable importance for the 69-Mev C data, and the

[14] F. Ajzenberg-Selove and T. Lauritsen, Nuclear Phys. **11**, 1 (1959).

TABLE III. Differential cross sections (in mb/sr) of oxygen for 87.5-Mev π^- mesons.

θ	Elastic	5-Mev inelastic	10-Mev inelastic
20±2.8°	230 ±11		
25±2.8°	162 ± 9		
30±2.8°	110 ± 8		
35±2.8°	75.3 ± 4.3		
40±2.8°	54.1 ± 2.5		
45±3.8°	27.2 ± 2.2		
50±3.8°	17.1 ± 0.9		
55±3.8°	8.4 ± 0.7		
60±3.8°	5.8 ± 1.1	0.97±0.99	1.10±0.86
65±3.8°	4.23± 0.71	0.56±0.62	1.00±0.51
70±3.8°	4.42± 0.60	0.37±0.57	0.35±0.90
75±4.5°	4.15± 0.62	[a]	1.10±0.33
80±4.5°	3.21± 0.88	0.05±0.81	1.48±0.58
85±4.5°	3.07± 0.55	0.78±0.45	2.05±0.41
90±4.5°	2.29± 0.42	1.58±0.47	[a]
95±4.5°	2.44± 0.46	0.20±0.44	2.61±0.44
100±4.5°	0.59± 0.33	2.10±0.48	1.44±0.72
105±4.5°	[a]	2.14±0.35	2.41±0.30
110±4.5°	0.29± 0.32	2.79±0.47	2.56±0.76
115±4.5°	[a]	2.69±0.38	2.62±0.34
120±4.5°	0.25± 0.32	2.54±0.46	1.44±0.87
130±4.5°	0.09± 0.45	3.93±0.82	2.55±0.86

[a] Unfolds to negative cross sections.

inelastic predominates for 87.5-Mev scattering from C and O to the extent that one can say only that the elastic cross section is $\lesssim 1$ mb/steradian. A qualitative comparison of the carbon curves, and the one of BRW, shows a similarity in the behavior of the 5- and 10-Mev inelastic scattering.

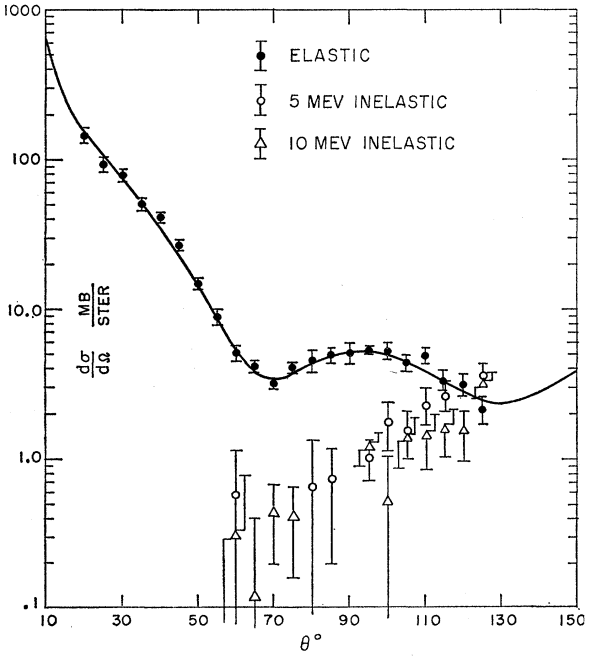

FIG. 6. 69.5-Mev π^--carbon scattering. Solid line is best-fitting modified Kisslinger model calculation with experimental angular resolution folded in. Nuclear parameters for best fit are $r_0=1.05\pm0.02$ fermis, $t=1.16\pm0.07$ fermis, $C_1=(-1.40\pm0.04)+i(-0.06\pm0.01)$, $C_0=(0.451\pm0.003)+i(-0.15\pm0.02)$.

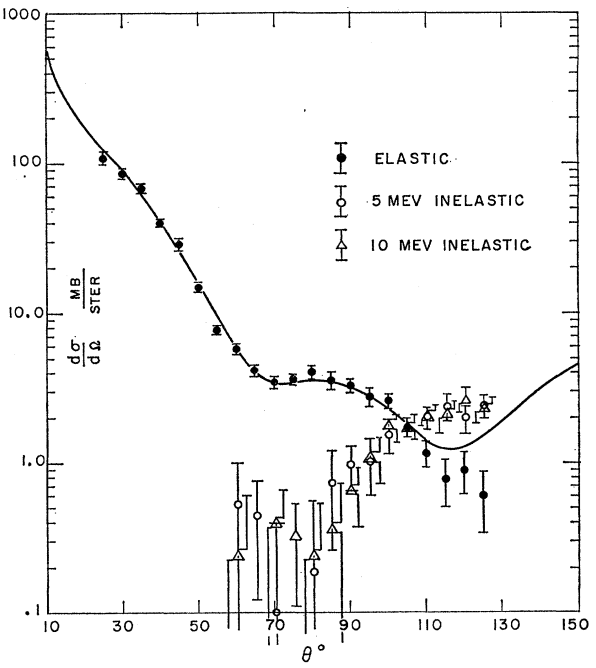

FIG. 7. 87.5-Mev π^--carbon scattering. Solid line is best-fitting modified Kisslinger model calculation with experimental angular resolution folded in. Nuclear parameters for best fit are $r_0=1.08$ f, $t=1.2$ f, $C_1=-1.1-0.15i$, $C_0=+0.35-0.15i$.

V. OPTICAL MODEL: CALCULATIONS AND DISCUSSION

Optical-model calculations were carried out to fit the three sets of elastic scattering data. For the most part, they were made using the modified Kisslinger optical-model equation discussed in BBR.

In the calculations of BBR a Fermi-type nuclear density distribution function was used,

$$\rho=\rho_0 F=\rho_0\left[1+\exp\left(\frac{r-R}{a}\right)\right]^{-1}, \tag{1}$$

where $R=r_0A^{\frac{1}{3}}$. A good fit was obtained using $r_0=1.08$ fermis and $a=0.25$ fermis for the 80-Mev π^- scattering from C and Li. Following the example of Cronin *et al.*,[15] we investigated the possibility of using the simpler "cubic" density function,

$$\begin{aligned} &F=1, && r<(R-\tfrac{1}{2}d)\\ &F=\tfrac{1}{2}-\tfrac{3}{2}\left(\frac{r-R}{d}\right)+2\left(\frac{r-R}{d}\right)^3, && |r-R|<\tfrac{1}{2}d\\ &F=0, && r>(R+\tfrac{1}{2}d). \end{aligned} \tag{2}$$

F and its first derivative are everywhere continuous for this form and the edge region is defined by

$$(R-\tfrac{1}{2}d)<r<(R+\tfrac{1}{2}d).$$

[15] J. W. Cronin, R. Cool, and A. Abashian, Phys. Rev. **107**, 1121 (1957).

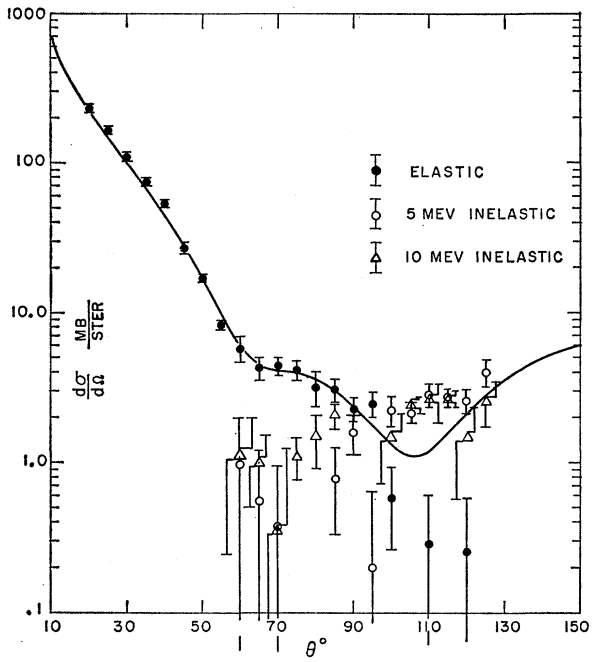

FIG. 8. 87.5-Mev π^--oxygen scattering. Solid line is best-fitting modified Kisslinger model calculation with experimental angular resolution folded in. Nuclear parameters for best fit are $r_0=1.08$ f, $t=1.2$ f, $C_1=-1.05-0.10i$, $C_0=+0.40-0.15i$.

This form also has the feature of a short-tail region. Keeping all other parameters the same in the modified Kisslinger optical model, it was found that the computed curves for $a=0.25$ fermis in form (1) and $d=2.0$ fermis in form (2) were almost identical. The two density functions are compared in Fig. 9 for these choices of a and d. It is seen that (1) is steeper near $r=R$, but approaches $F=0$ and $F=1$ less abruptly, giving comparable effective edge smearing. Equation (2) has been used for all the calculations reported here.

The Kisslinger theory uses the wave equation,

$$\nabla^2\psi+k_0^2\psi=U\psi=C_0k_0^2F\psi-C_1\nabla\cdot(F\nabla\psi)+U_c\psi, \quad (3)$$

where we include the Coulomb interaction term, U_c. The simply predicted constants, C_0 and C_1, are given by

$$C_l=\frac{-4\pi\rho_0}{k_0k_{\text{c.m.}}^2}\left[\frac{Z}{A}k_{\text{c.m.}}f_p+\frac{N}{A}k_{\text{c.m.}}f_n\right]_l, \quad l=0,1. \quad (4)$$

They arise from the s- and p-wave coherent scattering amplitudes for scattering from a unit volume of nuclear matter. ρ_0 is the nuclear density at $r=0$; $\hbar k_0$ is the incident pion momentum in the laboratory system; and $\hbar k_{\text{c.m.}}$ is the pion momentum in the center-of-mass system of the π and a single nucleon which is initially at rest in the laboratory system; f_p and f_n are single-nucleon scattering amplitudes. The effect of nuclear binding is implied in the definition of C_l inasmuch as one considers elastic scattering with respect to the nucleus as a whole. It is also assumed that the elemental pion-nucleon scattering amplitudes are proportional to k^2 for $l=1$ and constant for $l=0$, where $\hbar k$ is the effective momentum inside the nucleus. This assumption is reasonably valid for $l=0$ but is poor for $l=1$ if the effective momentum inside the nucleus is appreciably larger than that corresponding to $\sim$100-Mev kinetic energy. Figure 10 shows the predicted dependence of C_0 and C_1 on the meson laboratory kinetic energy using the equations of Chew and Low[16] for the momentum dependence of the δ_{33} phase shift and the linear forms for δ_1 and δ_3. (See for example Orear.[17]) The absolute value of $\mathrm{Re}(C_1)$ decreases rapidly and its sign changes in passing through the $(\frac{3}{2},\frac{3}{2})$ resonance at 193 Mev. One may regard $-Re(\nabla^2\psi/\psi)\equiv k_{\text{eff}}^2$ as a measure of the local value of k^2 inside the nucleus. If a value of C_1 corresponding to a meson kinetic energy of 70–100 Mev is used in (3) independent of k_{eff}^2, the quantity $(-C_1F\nabla^2\psi)$ on the right side can be combined with the $\nabla^2\psi$ on the left to give

$$\nabla^2\psi+k_0^2\psi=U'\psi=\frac{(C_0+C_1)k_0^2F\psi-C_1\nabla F\cdot\nabla\psi}{(1+C_1F)}, \quad (5)$$

neglecting for the moment the Coulomb term.

For $\mathrm{Re}(C_1)\approx-1.8$, the denominator "feedback" effect causes an increase in the right side of (5) as F increases from zero. For $F>0.6$, the sign of the real part of U' is actually reversed, thus corresponding to a repulsive potential. This range of variation of k_{eff}^2, however, is inconsistent with the choice of C_1 (from Fig. 10) and k_{eff}^2 should instead "saturate" due to the rapid change in $\mathrm{Re}(C_1)$ as the effective meson energy approaches 160–180 Mev. In principle, for each incident k_0^2 and F, one might choose a self-consistent value of C_1 which, using Fig. 10, leads to a $k_{\text{eff}}^2=-\mathrm{Re}(\nabla^2\psi/\psi)$ which predicts this C_1. This method has not been used so far because of its complexity. As indicated in BBR, $(1+C_1F)^{-1}$ has been replaced by $(1-C_1F)$ in the modified Kisslinger equation.

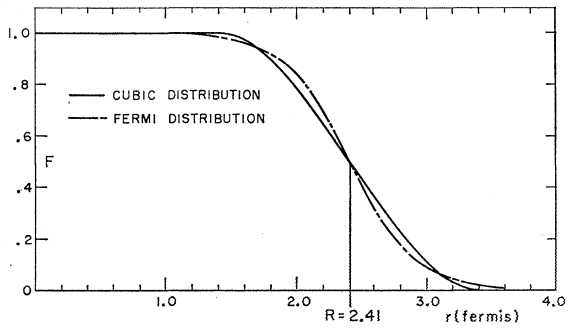

FIG. 9. Fermi and "cubic" nuclear density distributions which give the same prediction for 80-Mev π^--carbon scattering. $a=0.25$ f, $d=2.0$ f, and $R=2.41$ f ($r_0=1.05$ f).

[16] G. F. Chew and F. E. Low, *Proceedings of the Fifth Annual Rochester Conference on High-Energy Nuclear Physics* (Interscience Publishers, Inc., New York, 1955).

[17] J. Orear, Phys. Rev. **100**, 288 (1955).

It is relevant to consider the implications of this reasoning for the dependence of the best-fit $\mathrm{Re}(C_1)$ on k_0^2. The "saturation" of k_{eff}^2 at $\lesssim 160$ Mev suggests that C_1 be chosen for a k^2 between k_0^2 and the resonance. This implies that $|\mathrm{Re}(C_1)|$ be smaller than for k_0^2. Furthermore, as k_0^2 is decreased, the k^2 used to find $\mathrm{Re}(C_1)$ can be decreased leading to an increase in $|\mathrm{Re}(C_1)|$. In the best-fit matches shown in Figs. 6 and 7, this expectation is borne out since $C_1=(-1.1-0.15i)$ gives best fit at 87.5 Mev while $C_1=(-1.4-0.06i)$ gives best fit at 69.5 Mev. For reasons discussed in BBR, the best-fitting value for $\mathrm{Im}(C_1)$ is not expected to agree with the simple predictions of Fig. 10.

Kroll[18] has reexamined the "simplified" derivation of the Kisslinger equation, given in BBR, with emphasis on the difference between the effective field acting at a nucleon and the average field in analogy to the derivation of the classical Lorentz-Lorenz formula for an electromagnetic wave in a dielectric material.[19] Inclusion of this effect leads to the modified radial equation for given angular momentum, l,

$$\phi_l''+\left[k_0^2+\frac{l(l+1)}{r^2}\right]\phi_l = (1+\tfrac{2}{3}C_1F)^{-1}\left[k_0^2\left\{[C_1+C_0(1-\tfrac{1}{3}C_1F)] + \frac{(2E-V_c)V_c(1-\tfrac{1}{3}C_1F)}{(\hbar c k_0)^2}\right\}\phi_l - \frac{C_1F'(\phi_l'-\phi_l/r)}{1-\tfrac{1}{3}C_1F}\right], \quad (6)$$

where primes indicate differentiation with respect to r.

Since the factor $(1+C_1F)^{-1}$ of Eq. (15) of BBR has been replaced by $(1+\frac{2}{3}C_1F)^{-1}(1-\frac{1}{3}C_1F)$, the tendency of this factor to become singular and change sign has been reduced. It was thought that it might be possible to fit the experimental results with Eq. (6) without introduction of additional heuristic modifications. As has been previously reported,[20] this formula has been used in an attempt to fit the 80-Mev C data. Close to good agreement was obtained, but not as good as with the modified Kisslinger equation. Several attempts were made to fit the present data although a systematic study has not been made. The fits have not been as good as those obtained using the modified Kisslinger formula.

Equation (6) has a form somewhat intermediate between the original and modified Kisslinger formulas, although the surface term is given less weight in Eq. (6).

[18] N. M. Kroll (private communication).

[19] Max Born and Emil Wolf, *Principles of Optics* (Pergamon Press, New York, 1959), chap. 2.

[20] J. Rainwater, *Proceedings of the International Conference on the Nuclear Optical Model*, Florida State University Studies, No. 32, edited by A. E. S. Green, C. E. Porter, and D. S. Saxton (The Florida State University, Tallahassee, 1959).

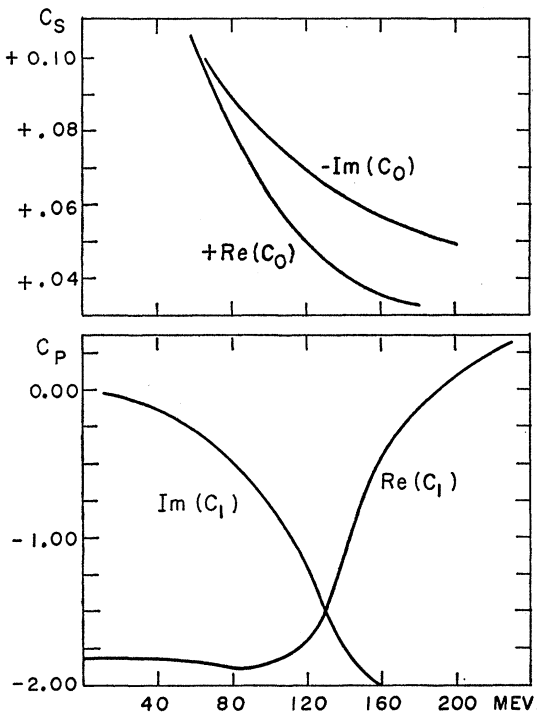

FIG. 10. Predicted energy dependence of C_0 and C_1 for carbon with $r_0=1.05$ f.

The arguments given for modifying the Kisslinger equation can also be applied to the Kroll equation, so the modified Kisslinger formula can also be regarded as a modified Kroll formula.

In fitting the calculated curves to the elastic scattering data, C_1 and C_0 (which are complex) and the nuclear size parameters, r_0 and d are varied to produce

TABLE IV. Nuclear parameters for best fit to data. The nuclear density function of Eq. (2) was used and $t=0.61d$ is the 10% density spacing.

69.5-Mev π^- mesons on carbon
$r_0=1.05\pm0.02$ fermis
$t=1.16\pm0.07$ fermis
$C_1=(-1.40\pm0.04)+i(-0.06\pm0.01)$
$C_0=(0.451\pm0.003)+i(-0.15\pm0.02)$
80-Mev π^- mesons on carbon (from BRW)
$r_0=1.08$ f
$t=1.2$ f
$C_1=-1.1-0.1i$
$C_0=+0.35-0.15i$
87.5-Mev π^- mesons on carbon
$r_0=1.08$ f
$t=1.2$ f
$C_1=-1.1-0.15i$
$C_0=+0.35-0.15i$
87.5-Mev π^- mesons on oxygen
$r_0=1.08$ f
$t=1.2$ f
$C_1=-1.05-0.10i$
$C_0=+0.40-0.15i$

good fits. In making the fits, the experimental angular resolution was folded into the theoretical curve before comparing. This made only a small difference but tended slightly to fill in the first minimum near 70° and shift it to a larger angle.

To provide a more quantitative check of the goodness of fit to the 69.5-Mev C data, a χ^2 analysis was performed to determine the values of the parameters giving the best fit and the amount by which they could be varied. Assuming the most general quadratic dependence of χ^2 on these six independent parameters, including cross terms, requires the determination of 28 coefficients, and therefore the determination of χ^2 for this many sets of parameters in the region of the minimum.

The best fitting values and the uncertainties found for each parameter are shown in Table IV along with values obtained for the other curves and for the 80-Mev π^--carbon data of BRW. Note that $t=0.61d$ is the fall-off parameter usually used; i.e., the distance from 0.9 to 0.1 times central density. The minimum χ^2 was 16.9 which compares well with the expected 16 ± 6 for 22 points and 6 parameters.

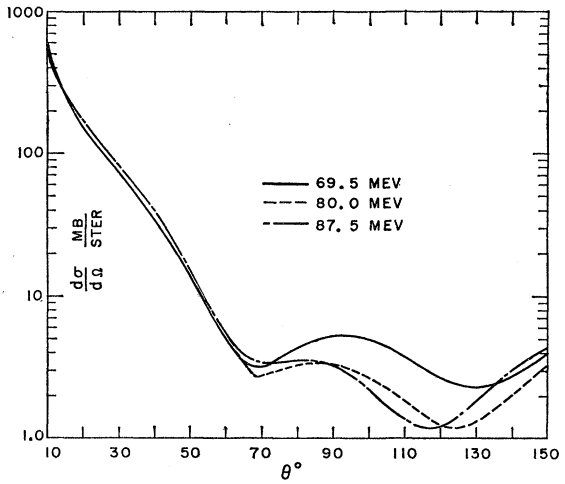

FIG. 11. Best-fitting modified Kisslinger calculations of π^--carbon scattering at 69.5, 80, and 87.5 Mev. Experimental angular resolution is not included.

VI. FURTHER DISCUSSION AND CONCLUSIONS

There are several regularities to be noticed in the elastic cross sections of this experiment and those of BRW. They are by and large the ones to be expected in diffraction scattering. Due to the improved technique, the diffraction patterns and the regularities in them are more clearly apparent than in previous experiments.

Born-approximation type calculations have had moderate success predicting π-nucleus scattering.[2–5] In particular, one can obtain back-angle cross sections which hold up. The qualitative features of the approximation are in agreement with the general trends observed in these experiments. The scattering amplitude in this approximation is of the form

$$\phi(\mathbf{q})=t_q A f(\mathbf{q}), \tag{7}$$

where $\mathbf{q}$ is the momentum transfer ($|\mathbf{q}|=2k\sin\frac{1}{2}\theta$), $\hbar k$ is incident pion momentum, t_q is the scattering amplitude from the "average" nucleon, and $f(\mathbf{q})$ is the nuclear form factor. In the quantitative application of this form, the scattering amplitude must be evaluated at the kinetic energy appropriate to the interior of the nucleus and account taken of the nucleon Fermi momentum, and of the fact that the scattering is elastic with respect to the nucleus as a whole. (See reference 3.) In this qualitative discussion, these refinements are neglected.

For scattering at energies well below the $(\frac{3}{2},\frac{3}{2})$ resonance, we have

$$t_q=B_0+B_1k_0^2\cos\theta, \tag{8}$$

where B_0 and B_1 (which take the place of C_0 and C_1) are nearly constant with pion momentum, k_0. B_0 gives the s-wave, and $B_1k_0^2\cos\theta$, the p-wave contribution to the scattering. (Spin-flip terms are omitted from t_q as not contributing to the coherent scattering.) For most of the small-angle region except close to the first minimum, $\phi(\mathbf{q})$ increases as k does, since at these energies the p-wave term dominates and t_q increases with k faster than $f(\mathbf{q})$ decreases. At small angles, the dependence of $f(\mathbf{q})$ on atomic number A is slow compared to the explicit term A, so ϕ increases with A. The diffraction pattern is determined for the most part by $f(\mathbf{q})$. Since f depends approximately on qR, or $qA^{\frac{1}{3}}$, an increase in either k or A shifts the pattern (in particular, the minima) to smaller angles.

Due to the signs of $\mathrm{Re}(B_0)$ and $\mathrm{Re}(B_1)$, $|t_q|$ has a minimum in the region of 70°–80° and then rises to values at large angles which exceed the forward angle values. This tendency to increase holds up the large-angle scattering against the general tendency of $f(\mathbf{q})$ to decrease in this region.

Figure 11 shows the modified-Kisslinger-model best fits to the three sets of carbon data superimposed for ease of comparison. In the small-angle region, there is a small but significant increase in cross section between the 69.5- and the 87.5-Mev data. The 80-Mev data cannot be distinguished from the 87.5-Mev data in this region but the predicted difference will be small in any case. There is no clear-cut shift in position of the first dip at ~70° with energy in either the experiment or the best-fit calculations. The second dip shows the expected regularity in the best-fit curves. The data do not fully show the second dip but can be said to be consistent with the predicted shift in this dip.

In the sequence Li, C, O, Al, Cu, the cross sections at small angles show a consistent increase with A. Also, the first and second diffraction dips occur at successively smaller angles. For Li, the second dip is not seen but it is obvious that it must appear at a larger angle than for

C if it occurs at all at this energy. As with C, the second dip in O is not fully seen, but the data are consistent with an appearance at the proper place. It must be noted, also, that the Al and Cu data included an unknown amount of inelastic scattering. This contribution is probably small for angles below the first dip.

Attempts of BBR to fit the 80-Mev π^--carbon data using an ordinary optical model potential $V+iW$ proportional to the nuclear density (corresponding to setting $C_1=0$) were unsuccessful. To fit the region below $\sim 60°$ required the larger nuclear radius parameter $r_0 \approx 1.4$ fermis. This may be understood qualitatively in that this model essentially uses an isotropic scattering for t_q. The dropoff of $\phi(\mathbf{q})$ as $\theta \rightarrow 60°$ must then come entirely from the nuclear form factor $f(\mathbf{q})$ without help from the shape of t_q. This requires a larger nuclear size.

The parameter r_0 is in good agreement with the electron scattering result, and the magnitudes and energy dependence of C_0 and C_1 are in reasonable agreement with expectation. The fact that the favored value of the nuclear edge thickness is only half that required to fit electron scattering data and other experiments possibly indicates a shortcoming of this theory which might not appear in a more elaborate self-consistent theory. The imaginary parts of C_0 and C_1 for best fit are not expected to agree well with the values calculated on the basis of pion scattering by free nucleons as discussed in BBR. Brueckner (reference 15 of BBR) has suggested that the absorption terms due to $l=1$ type nucleon scattering (C_1) should be proportional to the nuclear density and thus be included in the imaginary part of C_0. We see, in fact, that best fits are obtained having the absorption terms mainly associated with C_0 rather than C_1.

It would be of interest to see if agreement with experiment could be obtained using the Kroll equation, allowing $\mathrm{Re}(C_1)$ to vary with r in such a way as to give a self-consistent k_{eff}^2 at each r; i.e., such that the value of C_1 chosen gives rise to a k_{eff}^2 which is consistent with this choice.

In conclusion, we note that the modified Kisslinger formula gives good fits to the experimentally observed angular distribution for π^--meson elastic scattering from Li, C, and O at the energies measured by BRW and in the present study. Furthermore, the energy dependence of the parameters C_0 and C_1 for scattering from C at 69.5, 80, and 87.5 Mev is as expected. The nuclear radius required is in excellent agreement with that determined by electron scattering. Only the best-fitting choice of nuclear edge thickness differs from what is expected from other evidence.

ACKNOWLEDGMENT

We wish to express our sincere appreciation to the many people at the Nevis Cyclotron Laboratory whose cooperation insured the success of this experiment. We acknowledge the assistance given by Professor Norman Kroll in attempts to improve the theoretical basis for the optical model which we have used.